Synthesis and characterisation of the Rhenium-Molybdenum $Re_{0.6}Mo_{0.4}$ and Lanthanum-Strontium-Manganese-Oxide $La_{0.6}\,Sr_{0.4}\,MnO_3$ materials

Supervised by Prof. Fereidoon S. Razavi and Ms. Sara H. Monfared

Course: PHYS 5P81

Department of Physics

Brock University

Pratik Bhanuse

pb19xz@brocku.ca

December 10th, 2020

Abstract

The article discusses the two synthesis processes which were used to synthesis the Rhenium-Molybdenum and Lanthanum-Strontium-Manganese-Oxide superconductors. The detailed illustration of the various characterisation techniques were studies. These involved X-Ray Diffraction, Magnetisation, Resistivity measurements. The XRD analysis dictates the pervoskite structure of the LSMO sample and the MT curve and resistivity curve analysis of ReMo dictates the $T_C = 6.7K$. More detailed description of the synthesis and characterisation of ReMo and LSMO is provided below.

Keywords— ReMo, LSMO, XRD, SQUID, Resistivity, Superconductors

Acknowledgements

Throughout the writing of this report I have received a great deal of support and assistance.

I would first like to thank my supervisor, Professor Fereidoon Razavi, whose expertise was invaluable in formulating the research questions and methodology. Your insightful feedback pushed me to sharpen my thinking and brought my work to a higher level.

I would particularly like to single out the teaching assistant for this course Mr. Sara Monfared. Sara, I want to thank you for your patient support and for all questions and guidance I needed to complete my report.

I would also like to thank my course director, Professor Maureen Reedyk and my Professor David Crandle, for their valuable guidance throughout my studies. You provided me with the tools that I needed to choose the right direction and successfully complete my report.

In addition, I would like to thank my parents, Mrs. Laxmi Bhanuse and Mr. Bipinchandra Bhanuse and my sister Ms. Pratika Bhanuse for their wise counsel and sympathetic ear. You are always there for me. Finally, I could not have completed this report without the support of my friends, Mrs. Palak Patel, Mr. Sarvjeet Singh and my partner in crime Mr. Zeyu Li, who provided stimulating discussions as well as happy distractions to rest my mind outside of my research.

Contents

List of Figures

List of Tables

1 Introduction

1.1 ReMo

Molybdenum-Rhenium (Mo-Re) is a disordered superconducting alloy with noble surface chemistry and a relatively high transition temperature. Molybdenum-Rhenium (Mo-Re) is an attractive superconducting alloy which has been explored as early as the 1960s [Lerner et al., 1967, Yasaitis and Rose, 1975, Andreone et al., 1989]. It is a Type II superconductor which means that besides being mechanically harder than Type I superconductors, they exhibit much higher critical magnetic fields. Some other examples of Type II super conductors are NbTi, PbMoS, etc.

Molybdenum-47.5%-Rhenium Wire is used in welding, electronics and wire mesh grids for the aerospace industries. Alloying Rhenium with Molybdenum adds both ductility and strength to wire products. Molybdenum-Rhenium alloys serve a wide range of applications in electronics, furnace, joining, and aerospace industries. Alloying Rhenium and Molybdenum increases both strength and ductility to plate sheet and foil products. Molybdenum-Rhenium foil and sheet are typically used in the production of cathode emitters and a variety of other electronic product applications. Molybdenum-Rhenium is also used to upgrade conventional applications in furnace parts and tooling along with feed stocks for the electronic and semiconductor industries.

Recently, there has been a renewed interest in ReMo superconductors due to its electrical and mechanical properties [Singh et al., 2014]. Depending on the alloying ratio and film deposition temperatures, thin films of Mo-Re have shown superconducting transition temperatures (Tc) ranging from 8 K to 13 K and residual resistance ratios RRR ≈ 1 indicating their highly disordered nature.

1.2 LSMO

$La_{0.6}\,Sr_{0.4}\,MnO_3$ (LSMO) perovskite structure is a colossal microwave-adsorbent magnetoresistance (CMR) with high absorption and broad frequency band. LSMO 's fascinating magnetic and electronic properties have been widely used in magnetic tunnelling junctions manufacturing. LSMO is black in colour and has a density of around $6.5 g/cm^3$. The actual density will vary depending on the method of processing and the actual stoichiometry. LSMO is primarily an electronic conductor, with near - 1 transference number.

This material is widely used in commercially manufactured solid oxide fuel cells (SOFCs) [Ormerod, 2003] as a cathode substrate since it has strong electrical conductivity at higher tem-

peratures and its thermal expansion coefficient is well balanced with yttria-stabilised zirconia (YSZ) [Ray et al., 2000], a popular material for SOFC electrolytes. LSMO acts as a semi-metal, suggesting its possible use in spintronics. It exhibits an effect of colossal magnetoresistance. Over its Curie temperature (approx. 350 K) Jahn-Teller polarons are formed; the ability of the material to conduct electricity depends on the presence of the polarons [Kolb, 2005].

2 Synthesis methodology

2.1 Re-Mo synthesis - Arc Melting

Arc Melting is used to heat metals, usually for alloys formation. Heating is by an electric arc produced between a tungsten electrode and metals put in a copper core depression (crucible). The chamber is evacuated in the vacuum arc melting and then packed up with argon air. Hence, melting takes place in the argon presence atmospheric condition [Kabiri et al., 2012].

Preparation of the Molybdenum - Rhenium alloy can be done by the arc melting process [Shang et al., 2019]. Though some research articles suggest that the best Re-Mo alloys can be made by using 40-50 % wt Re to Mo. Also, two commercial alloys have the compositions Mo - 41 wt % Re and Mo - 47.5 wt % Re [Carlen, 1995].

The phase transition occurring during the synthesis of the sample is described in the below chemical phase equation:

$$liquid \rightarrow bcc - W + \beta - CrFe \tag{1}$$

$$liquid + hcp - Mg \rightarrow \beta - CrFe \tag{2}$$

To synthesise the pure β-CrFe form, the first reaction was prevented by interrupting the heating immediately after both the Re and Mo metals were melted. As for the phase α-Mn, this can not be synthesised through arc melting, because no such phase occurs during the cooling of the liquid mixture. But this step involves two other reactions which are as follows:

$$\beta - CrFe + hcp - Mg \rightarrow \alpha - Mn \tag{3}$$

$$\beta - CrFe \rightarrow bcc - W + \alpha - Mn \tag{4}$$

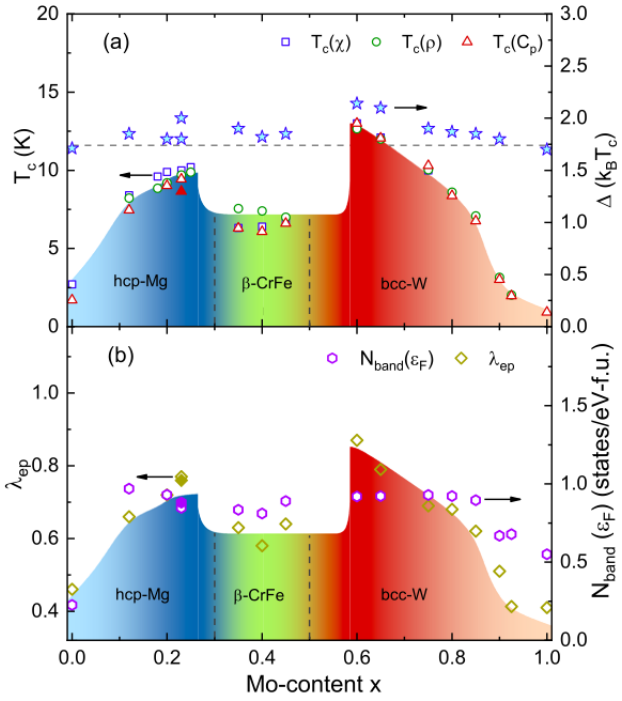

Figure 1: Binary phase diagram for Re-Mo synthesis [Shang et al., 2019]

Seeing as, both the situations have solid-state reactions involvement. The pure phase α-Mn can be procured by annealing the melted Re and Mo metals at 1400°C [Shang et al., 2019].

Remark: In order to improve homogenity, sample should be flipped and remelted multiple times (approximately six) [Stewart and Giorgi, 1978].

2.1.1 Calculation for raw material

As, we have considered the mode of preparation to be the arc melting [Kabiri et al., 2012, Timmons, 1977]. Thus, the calculation for the amount of raw materials required in synthesising 2.69 grams of $Re_{0.6}$ $Mo_{0.4}$ is done as follows:

- Atomic mass of Rhenium (Re) = 186.2 g/mol
- Atomic mass of Molybdenum (Mo) = 95.95 g/mol

Thus, molecular mass of our sample i.e., $Re_{0.6}$ $Mo_{0.4}$ is:

$$186.2 \times 0.6 + 95.95 \times 0.4 = 150.1 g/mol \tag{5}$$

Now, we need 2.69 mg (0.00269) of the sample thus the dividing factor to the molecular mass of our sample comes out to be 55.80. Hence, to get an exact amount of Re wire and Mo sheet can be calculated as:

$$Re = \left(\frac{186.2 \times 0.6}{55.8}\right) = 0.002mg \tag{6}$$

$$Mo = \left(\frac{95.95 \times 0.4}{55.8}\right) = 0.0068mg \tag{7}$$

Thus, in order to prepare 2.69 mg of $Re_{0.6}$ $Mo_{0.4}$ we require, 2.0 mg of Re wire and 0.6878 mg of Mo sheet.

Remarks: Although, these calculations are very ideal, thus, there might be some loss of end sample during the preparation process so one must keep in mind to have a little extra.

2.2 LSMO synthesis

$La_{0.6}\,Sr_{0.4}\,MnO_3$ (LSMO) perovskite structure is a colossal microwave-adsorbent magnetoresistance (CMR) with high absorption and broad frequency band. LSMO 's fascinating magnetic and electronic properties have been widely used in magnetic tunnelling junctions manufacturing. LSMO is black in colour and has a density of around $6.5g/cm^3$. The actual density will vary depending on the method of processing and the actual stoichiometry. LSMO is primarily an electronic conductor, with near - 1 transference number.

This material is widely used in commercially manufactured solid oxide fuel cells (SOFCs) [Ormerod, 2003] as a cathode substrate since it has strong electrical conductivity at higher temperatures and its thermal expansion coefficient is well balanced with yttria-stabilised zirconia (YSZ) [Ray et al., 2000], a popular material for SOFC electrolytes. LSMO acts as a semi-metal, suggesting its possible use in spintronics. It exhibits an effect of colossal magnetoresistance. Over its Curie temperature (approx. 350 K) Jahn-Teller polarons are formed; the ability of the material to conduct electricity depends on the presence of the polarons [Kolb, 2005].

The preparation of the LSMO sample can be done by various methods. Some of them are as Sol-Gel, Solid state reaction and Pulsed Laser Deposition. A combination of these methods can be used to develop a thin film sample of LSMO on a particular substrate. Lets dive in describing these methods individually.

2.2.1 Sol Gel

Sols are colloidal particle dispersion within a liquid. Colloids are solid particles with 1-100 nm diameters. A gel is an interconnected, stiff network with submicrometer-dimensional pores and polymeric chains with an average length greater than a micrometre. The goal of sol-gel processing is to control the structure of a material on a nanometer scale from the earliest stages of processing [Hench and West, 1990].

2.2.2 Solid State Reaction

The most widely used method of preparing polycrystalline solids from a mixture of solid starting materials is the solid-state reaction route. Solids do not react together over normal time scales at room temperature, and it is necessary to heat them up to much higher temperatures, often up to 1000 to 1500 ° C, in order for the reaction to occur at a considerable rate. The factors on which the feasibility and rate of a solid state reaction depend include the reaction conditions, the structural properties of the reactants, the surface area of the solids, their reactivity and the associated thermodynamic free energy change [West, 2014]

2.2.3 Pulsed Laser Deposition (PLD)

Pulsed laser deposition (PLD) (refer to Figure 2)is a versatile process for several purposes. As the energy source is located outside the chamber with this procedure, the use of ultra-high vacuum (UHV) as well as ambient gas is possible. This enables all sorts of different materials to be deposited together with a stoichiometry transition between the target and substrate [Krebs et al., 2003, Smith and Turner, 1965].

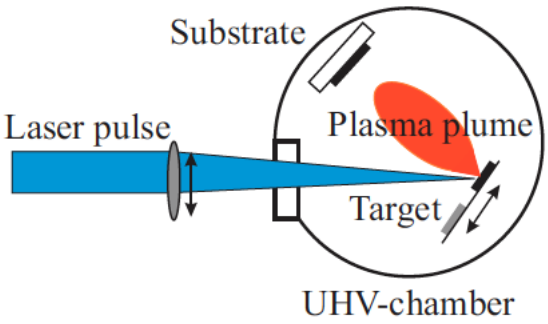

Figure 2: Schematic diagram of a typical laser deposition set-up [Krebs et al., 2003]

3 Results

3.1 X-Ray Diffraction (XRD) analysis

X-ray diffraction is a powerful nondestructive technique for characterising crystalline materials. It provides information on structures, phases, preferred crystal orientations (texture), and other structural parameters, such as average grain size, crystallinity, strain, and crystal defects. XRD peaks are produced by constructive interference of a monochromatic beam of X-rays scattered at specific angles from each set of lattice planes in a sample. The peak intensities are determined by the atomic positions within the lattice planes. Consequently, the XRD pattern is the fingerprint of periodic atomic arrangements in a given material. An online search of a standard database for X-ray powder diffraction patterns enables quick phase identification for a large variety of crystalline samples [Kohli and Mittal, 2018].

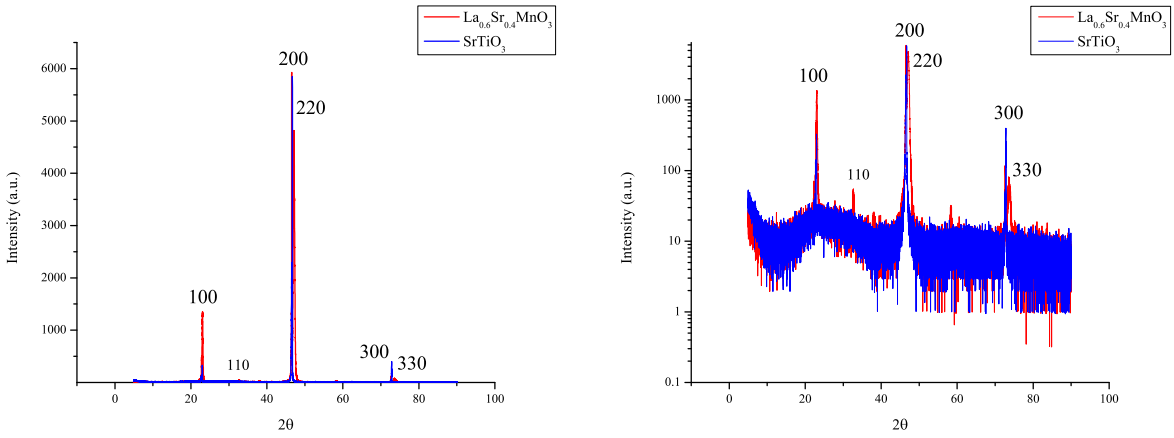

(a) Linear curve

(b) logarithmic curve

Figure 3: LSMO X-Ray Diffraction curve

As shown in the XRD analysis (refer Figure 3), there are two curves: one for the sample (denoted in red) and one for the substrate $SiTiO_3$ aka. STO (denoted in blue). In Figure 3a and Figure 3b we can see the two very distinguishable peaks at 23.19° and 46.77° respectively. Whilst, two weak peak at 32.67° and 73.75°.

These specific peaks are signatory authentication of the pseudocubic perovskite structure (refer Figure 4). One can also calculate the lattice parameters from the XRD data. The high (001)-orientation of the LSMO thin film on the Si (001) substrate is known to be a self-textured growth that satisfies the minimum surface energy requirements [Rao and Yu, 2011].

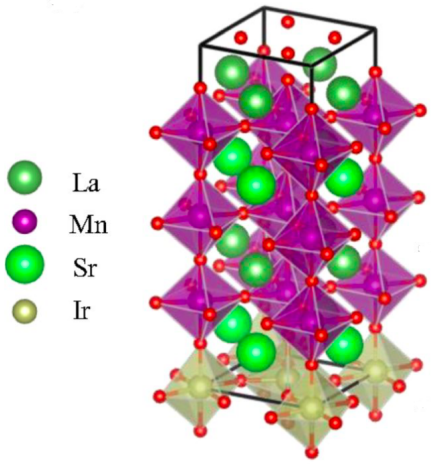

Figure 4: Perovskite Structure [Yi et al., 2016]

Peaks	2θ	Material
100	23.19°	STO
110	32.67°	LSMO
200	46.77°	STO
220	47.11°	LSMO
300	73.75°	STO
330	73.66°	LSMO

Table 1: XRD peaks table

3.2 Magnetic studies - SQUID analysis

Magnetometers based on a superconducting quantum interference device (SQUID) are capable of resolving $10-15$ T sized changes in the magnetic field. We use a SQUID magnetometer from Quantum Design (MPMS-XL5) to measure the static magnetisation of samples at various applied fields with constant temperature (isothermal), $M_{DC}(\mu_0 H)$, and at various temperatures with a constant applied field, $M_{DC}(T)$ (or $\chi_{DC}(T) = M_{DC}(T)/\mu_0 H$). The SQUID device within the magnetometer consists of a closed superconducting loop with two Josephson junctions in the current path of the loop. A direct result of the quantisation of magnetic flux coupled with the non-linear behaviour of the Josephson junction allows for a SQUID magnetometer to resolve minute changes of the external magnetic field that are induced by a magnetic sample passing through the SQUID, and stay operational in large applied fields [Lin et al., 2018].

The Figure 5 is a visual representation of the magnetic behaviour of the $Re_{0.6}Mo_{0.4}$ superconductor. If we look at the Figure 5b we get to see that the magnetisation drops at 6.35 K which represents the transition temperature (T_C) for $Re_{0.6}Mo_{0.4}$ [Patel et al., 2019]. Physically speaking

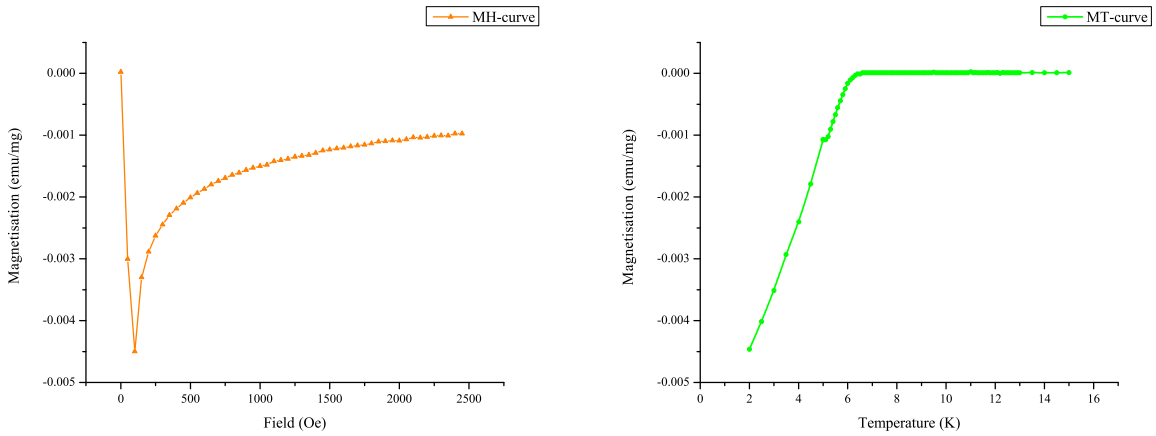

(a) Magnetisation vs Magnetic field curve (b) Magnetisation vs Temperature curve

Figure 5: Magnetisation study of $Re_{0.6}Mo_{0.4}$

this represents the transfiguration of magnetic properties of $Re_{0.6}Mo_{0.4}$. Above T_C the sample displays metallic behaviour whilst, below T_C the sample demonstrates the superconductive behaviour. Further detailed authentication of the transition temperature is illustrated in below section 6.

In the Figure 5a we study the variation of magnetisation with respect to applied external magnetic field. In this we observe the material displays diamagnetic behaviour, as we observe under the influence of magnetic field the magnetisation is grown to negative. The sudden drop in magnetisation is very prominently dominated following the gradual increment in magnetisation along the increase in magnetic field. This could be implicated due to the alignment of domains in the sample, which is under the strong influence of changing external magnetic field. In order to understand the magnetism of the material we need to further magnetic susceptibility analysis.

3.3 Resistivity measurement analysis

In general, the electrical resistivity is inversely proportional to the carrier density and the carrier mobility. A change in the nature of the chemical binding primarily alters the carrier density, and the structural changes alter the carrier mobility [Singh, 2013]. Four sharp probes are placed on a flat surface of the material to be measured (Fig.7). The current is passed through the two outer electrodes, and the floating potential is measured across the inner pair. If the flat surface on which the probes rest is adequately large, it may be considered to be a semi-infinite volume. To prevent minority carrier injection and make good contacts, the surface on which the probes rest,

maybe mechanically lapped.

3.3.1 ReMo resistivity

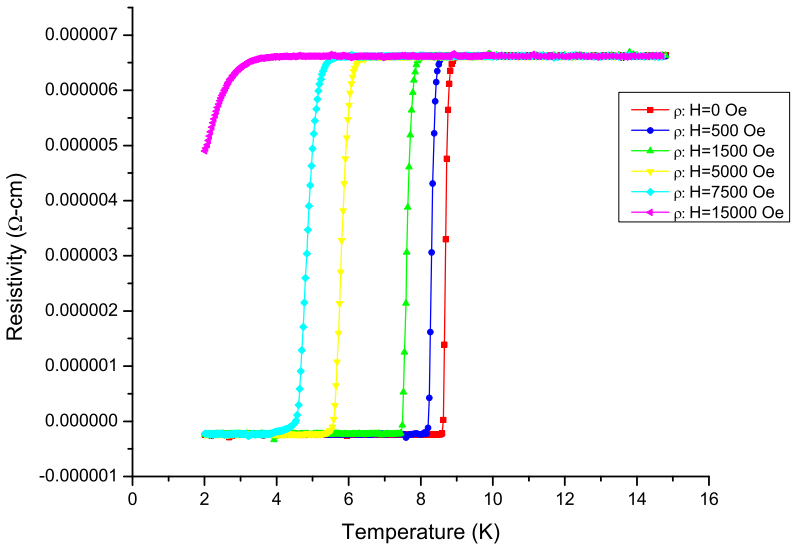

Figure 6: ReMo resistivity curve

In the shown Figure 6 we can see the relationship between the resistivity and the temperature for the $Re_{0.6}Mo_{0.4}$ sample. The measure was done for the temperature ranging from 2K to 16K to get a specified view of the curie temperature measurements for various external magnetic field. If observed carefully we can notice that up until approximately 10K we find the sample to display metallic behaviour. Whereas, below which the sample behaves like a superconductor. Below given Table 2, illustrates the variation in the transition temperature (T_C) with respect to the applied external magnetic field. We also found that as the external magnetic field was increased the transition temperature was decreased, which indicates towards the presence of the inverse relationship between both. Also, one can observe with varying the concentration of the Molybdenum that particularly $Re_{0.6}Mo_{0.4}$ sample is in the β-CrFe phase (refer to Figure 1). Which also indicates the decrement in the electrical resistivity compared to other phases. Where as in case of the magnetic field H = 15000 Oe = 1.5T we observe that the material doesn't make the transition into the superconducting phase.

External Magnetic field (H) (Oe)	Transition Temperature (T_C) (K)
0	8.59
500	8.17
1500	7.53
5000	5.54
7500	4.45

Table 2: Relation between external magnetic field and transition temperature (T_C) for $Re_{0.6}Mo_{0.4}$ sample.

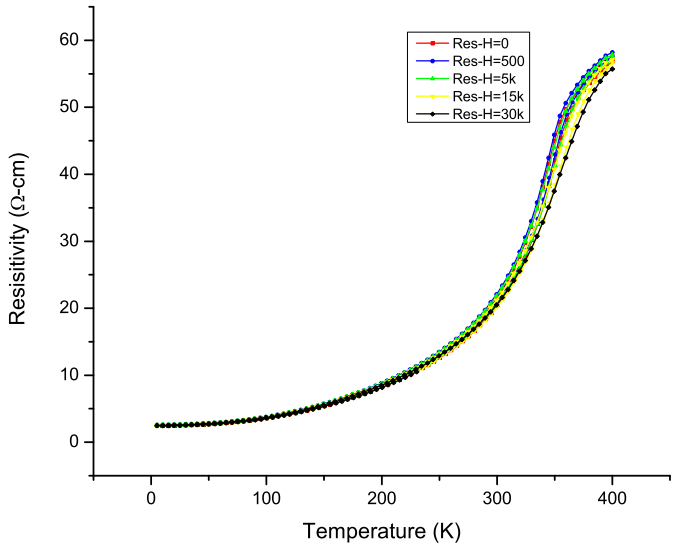

Figure 7: LSMO resistivity curve

3.3.2 LSMO resistivity

In the Figure 7 we have shown the resistivity behaviour of the $La_{0.6}\,Sr_{0.4}\,MnO_3$ material with respect with temperature which is influenced in various external magnetic field values. The data was acquired in a very strategic pattern of going high to low temperature and then low to high. Where the temperature was ranging from 0K to 373K. Through a rough examination of the resistivity curve (refer Figure 7) we identify that the curve inclines to show a potential transition point beyond the 373K. Which indeed needs a solid evidence which can be acquired through the further analysis of the material. These analysis are needed to be performed prominently beyond the 373K in order to get the transitioning phase of the materials.

4 Conclusion

In summary, we successfully synthesised ReMo and LSMO samples and various characterisation were performed to understand its physical, magnetic and electrical properties. It was found that ReMo sample displays the superconducting properties at around $T_C = 6.7K$ as mentioned in the section 3.2 which is also validated using the resistivity measurements mentioned in the section 3.3.1. Also by the further examination of the MH curve in Figure 5a, we identify the potential magnetic domain behaviour, which indeed needs further detailed inspection. In the XRD analysis of $La_{0.6}Sr_{0.4}MnO_3$ we identified the structure to be Perovskite structure and were success in explicitly distinguishing between the LSMO (sample) peaks and the STO (substrate) peaks. Lastly, in the resistivity measurement analysis, we identified variation of transition temperature with respect to the various applied external magnetic field. Also as mentioned in the section 3.3.1 we correlate the transition temperature obtained from MT curve (refer Figure 5b) and the one from the 0 Oe field in Figure 6. Whereas in the examination of the LSMO resistivity we identify that the transition temperature is due to be observed beyond the 373 K. Thus, it will require further detailed analysis with higher temperature.

References

[Andreone et al., 1989] Andreone, A., Barone, A., Di Chiara, A., Mascolo, G., Palmieri, V., Peluso, G., and Di Uccio, U. S. (1989). Mo-re superconducting thin films by single target magnetron sputtering. *IEEE transactions on magnetics*, 25(2):1972–1975.

[Carlen, 1995] Carlen, J. C. (1995). Molybdenum-rhenium alloy. US Patent 5,437,744.

[Hench and West, 1990] Hench, L. L. and West, J. K. (1990). The sol-gel process. *Chemical reviews*, 90(1):33–72.

[Kabiri et al., 2012] Kabiri, Y., Kermanpur, A., and Foroozmehr, A. (2012). Comparative study on microstructure and homogeneity of niti shape memory alloy produced by copper boat induction melting and conventional vacuum arc melting. *Vacuum*, 86(8):1073–1077.

[Kohli and Mittal, 2018] Kohli, R. and Mittal, K. (2018). *Developments in Surface Contamination and Cleaning: Applications of Cleaning Techniques: Volume 11*, volume 11. Elsevier.

[Kolb, 2005] Kolb, R. (2005). It's over: Uc wins lab contract on merit.

[Krebs et al., 2003] Krebs, H.-U., Weisheit, M., Faupel, J., Süske, E., Scharf, T., Fuhse, C., Störmer, M., Sturm, K., Seibt, M., Kijewski, H., et al. (2003). Pulsed laser deposition (pld)–a versatile thin film technique. In *Advances in Solid State Physics*, pages 505–518. Springer.

[Lerner et al., 1967] Lerner, E., Daunt, J., and Maxwell, E. (1967). Magnetic properties of superconducting mo-re alloys. *Physical Review*, 153(2):487.

[Lin et al., 2018] Lin, K.-W., Ouyang, C. H., and van Lierop, J. (2018). Using ion-beam-assisted deposition and ion implantation for the rational control of nanomagnetism in thin film and nanostructured systems. In *Solid State Physics*, volume 69, pages 1–45. Elsevier.

[Ormerod, 2003] Ormerod, R. M. (2003). Solid oxide fuel cells. *Chemical Society Reviews*, 32(1):17–28.

[Patel et al., 2019] Patel, D., Kim, S.-H., Qiu, W., Maeda, M., Matsumoto, A., Nishijima, G., Kumakura, H., Choi, S., and Kim, J. H. (2019). Niobium-titanium (nb-ti) superconducting joints for persistent-mode operation. *Scientific reports*, 9(1):1–7.

[Rao and Yu, 2011] Rao, W. and Yu, J. (2011). The structural and morphology of (la0. 7sr0. 3) mno3 thin films prepared by pulsed laser deposition. In *Advanced Materials Research*, volume 150, pages 908–911. Trans Tech Publ.

[Ray et al., 2000] Ray, J. C., Pati, R. K., and Pramanik, P. (2000). Chemical synthesis and structural characterization of nanocrystalline powders of pure zirconia and yttria stabilized zirconia (ysz). *Journal of the European Ceramic Society*, 20(9):1289–1295.

[Shang et al., 2019] Shang, T., Gawryluk, D. J., Verezhak, J. A., Pomjakushina, E., Shi, M., Medarde, M., Mesot, J., and Shiroka, T. (2019). Structure and superconductivity in the binary re 1- x mo x alloys. *Physical Review Materials*, 3(2):024801.

[Singh et al., 2014] Singh, V., Schneider, B. H., Bosman, S. J., Merkx, E. P., and Steele, G. A. (2014). Molybdenum-rhenium alloy based high-q superconducting microwave resonators. *Applied Physics Letters*, 105(22):222601.

[Singh, 2013] Singh, Y. (2013). Electrical resistivity measurements: a review. In *International journal of modern physics: Conference series*, volume 22, pages 745–756. World Scientific.

[Smith and Turner, 1965] Smith, H. M. and Turner, A. (1965). Vacuum deposited thin films using a ruby laser. *Applied Optics*, 4(1):147–148.

[Stewart and Giorgi, 1978] Stewart, G. and Giorgi, A. (1978). A search for strong coupling superconductivity. *Solid State Communications*, 28(12):969–972.

[Timmons, 1977] Timmons, G. A. (1977). Semi-consumable electrode vacuum arc melting process for producing binary alloys. US Patent 4,007,770.

[West, 2014] West, A. R. (2014). *Solid state chemistry and its applications*. John Wiley & Sons.

[Yasaitis and Rose, 1975] Yasaitis, J. and Rose, R. (1975). Microwave surface resistance of a superconducting mo-re alloy. *IEEE Transactions on Magnetics*, 11(2):434–436.

[Yi et al., 2016] Yi, D., Liu, J., Hsu, S.-L., Zhang, L., Choi, Y., Kim, J.-W., Chen, Z., Clarkson, J. D., Serrao, C. R., Arenholz, E., et al. (2016). Atomic-scale control of magnetic anisotropy via novel spin–orbit coupling effect in la2/3sr1/3mno3/sriro3 superlattices. *Proceedings of the National Academy of Sciences*, 113(23):6397–6402.